A modified in-plane constitutive model for paperboard

Marcus Pfeiffer[1], Stefan Kolling[1], Philipp Stein[2], Wilken Franke[2]

[1]Institute of Mechanics and Materials, Technische Hochschule Mittelhessen, Giessen
[2]Institute for Production Engineering and Forming Machines, Technische Universität Darmstadt

1 Abstract

In the present work, a continuum modelling approach for the in-plane orthotropic elastic-plastic material behaviour of paperboard is combined with Continuum Damage Mechanics (CDM). Bulge experiments were performed, and the simulation results of the present approach are compared to ***MAT_PAPER**. A CDM formulation is used to account for softening effects and a numerical study is performed to assess the effect of damage evolution on the resulting strains in bulge test simulations.

2 Introduction

Paper and paperboard are commonly used in the printing, packaging and hygiene industry. But paperboard also offers notable mechanical properties [1] in combination with recyclability. Paperboard is already used in architecture where the most discussed works might be those of Shigeru Ban [12]. A reliable prediction of the material response is necessary when paperboard is used in engineering applications. Here, finite element simulations are a preferred tool in today's CAE workflow.
Paperboard can be described macroscopically as an orthotropic material. A high stiffness is obtained in the so-called machine direction (MD) as the fibers are preferably aligned into the direction of the manufacturing process. The perpendicular in-plane direction is called cross-direction (CD) and the z-direction (ZD) is aligned normal to the paperboard plane. A number of continuum modelling approaches were already developed for paperboard, see e.g. [2, 3, 4, 5, 6, 7]. Some of them [2, 4] use the classical yield criterion presented in [8] originally proposed for polycrystalline materials. In [3] a yield criterion is suggested which under multiaxial loading [7, 11] shows reasonable model predictions where all necessary parameters were obtained experimentally from uniaxial tests. For further improvement of the simulation with paperboard materials, in the present work a modified approach is used to account for experimental results of bulge experiments. The model is extended using CDM and the CDM framework is presented here in detail.
Paperboard is known to exhibit damage effects [2, 13]. Fig. 1 shows uniaxial tensile tests of samples tested in MD, which were pre-strained in CD, compared to reference experiments. A free span size of 40 x 10 mm² was used at a thickness of 0.55 mm. To pre-strain the samples a large test specimen of 300 x 60 mm² was loaded in CD until fracture occurred and from which the samples were cut out. Similar tests were performed in [21]. A set of five samples was tested after pre-straining. The elastic stiffness of the pre-strained samples is reduced by about 25 %. To account for multiaxial softening phenomena using a continuum modeling approach CDM is utilized in the present work. Bulge experiments were performed and the occurrence of damage and the influence on resulting strains in these tests is investigated by a numerical study. To overcome localization effects in numerical simulations a viscous regularization is used [22].

3 Continuum damage mechanics

3.1 Notation

In the following and according to Cartesian coordinates 2nd order tensors are denoted as

$$\underline{A} = A_{ij}\,\vec{e}_i \otimes \vec{e}_j \tag{1}$$

and the scalar product of two 2nd order tensors is defined as

$$\underline{A} : \underline{B} = A_{ij}B_{ij}. \tag{2}$$

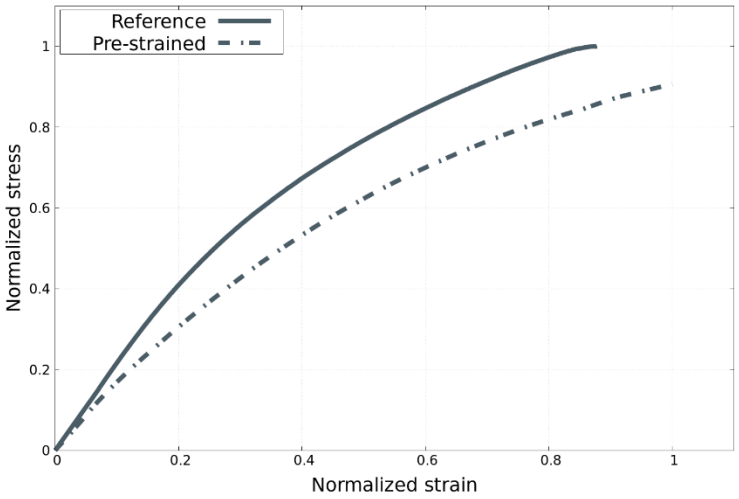

Fig. 1: Damage evolution due to pre-straining in lateral in-plane direction in comparison to undamaged samples.

Forth order tensors are denoted by a double underline, e.g.

$$\underline{\underline{C}} = C_{ijkl}\vec{e}_i \otimes \vec{e}_j \otimes \vec{e}_k \otimes \vec{e}_l. \tag{3}$$

3.2 General Framework

In the present work the virtual undamaged configuration is utilized which is a basic principle in CDM. The stress in this configuration is higher as no damage effects such as micro-cracking are present and the undamaged Young's modulus is recovered. The transformation of stress to the virtual configuration is given as [14, 18]

$$\overline{\underline{\sigma}} = \left(\underline{1} - \underline{D}\right)^{-\frac{1}{2}} \underline{\sigma} \left(\underline{1} - \underline{D}\right)^{-\frac{1}{2}} \tag{4}$$

with the Cauchy stress $\underline{\sigma}$ acting in the actual material body, the 2nd order identity tensor $\underline{1}$ and the 2nd order damage tensor $\underline{D}$. Quantities in the virtual configuration are in the following denoted with an overbar. Utilizing the orthonormal material coordinate system yields a damage tensor

$$\underline{D} = D_i\, \vec{e}_i \otimes \vec{e}_i, i = 1,2,3 \tag{5}$$

with a damage variable defined for each material direction. The material coordinate system will be used in the following as the reference coordinate system and necessary coordinate transformations should be performed in a preliminary step.
Eq. (4) yields a symmetric stress tensor $\overline{\underline{\sigma}}$ in the virtual undamaged configuration. To simplify further calculations a linear mapping with a 4th order tensor [15] is obtained from Eq. (4)

$$\overline{\underline{\sigma}} = \underline{\underline{M}} : \underline{\sigma}. \tag{6}$$

In matrix notation the so called damage effect tensor $\underline{\underline{M}}$ [18, 20] is given as

$$M = diag\left((\phi_1)^2, (\phi_2)^2, (\phi_3)^2, \frac{\phi_1\phi_2}{2}, \frac{\phi_2\phi_3}{2}, \frac{\phi_3\phi_1}{2}\right) \tag{7}$$

where $\phi_i = (1 - D_i)^{-1/2}$.
In the present work the strains in the actual and virtual configuration are assumed to be equal [16]. Other assumptions are also possible as e.g. an equivalence of total energies. Strain equivalence yields a simple damage and plastic iteration scheme as these iterations can be performed separately. Assuming strain equivalence yields

$$\underline{\varepsilon} = \underline{\underline{S}}^{D} : \underline{\sigma} = \underline{\underline{S}}^{0} : \underline{\bar{\sigma}} = \underline{\underline{S}}^{0} : \underline{\underline{M}} : \underline{\sigma} \tag{8}$$

where $\underline{\underline{S}}$ denotes the compliance and the superscripts 0 and *D* respectively denote an undamaged and damaged quantity. From Eq. (8) $\underline{\underline{M}}$ can be calculated as

$$\underline{\underline{S}}^{D} = \underline{\underline{S}}^{0} : \underline{\underline{M}}. \tag{9}$$

It is evident from Eq. (9) that this leads to a non-symmetric damaged compliance tensor. To overcome this issue a symmetrized damaged compliance tensor

$$\underline{\underline{S}}^{D^*} = \frac{1}{2}\left[\underline{\underline{S}}^{0} : \underline{\underline{M}} + \underline{\underline{M}} : \underline{\underline{S}}^{0}\right] \tag{10}$$

is introduced [18] which consequently yields a new damage effect tensor

$$\underline{\underline{M}}^{*} = \underline{\underline{S}}^{0-1} : \underline{\underline{S}}^{D^*} = \frac{1}{2}\left[\underline{\underline{M}} + \underline{\underline{S}}^{0-1} : \underline{\underline{M}}^{T} : \underline{\underline{S}}^{0}\right]. \tag{11}$$

3.3 Thermodynamics

In the present work the strain energy of the damaged continuum is assumed as [16]

$$\psi = \frac{1}{2}\underline{\varepsilon} : \underline{\underline{C}}(D^*) : \underline{\varepsilon} + \underline{\sigma}^{p} : \underline{\varepsilon} + \Xi(\alpha) \tag{12}$$

where the plastic stress $\underline{\sigma}^{p}$ is introduced as well as the plastic potential Ξ and

$$\underline{\underline{C}}(D^*) = \left(\underline{\underline{S}}^{D^*}\right)^{-1}. \tag{13}$$

By using the Clausius-Duhem inequality and applying standard arguments the Cauchy stress is given as

$$\frac{\partial \psi}{\partial \underline{\varepsilon}} = \underline{\sigma} = \underline{\underline{C}}(D^*) : \underline{\varepsilon} + \underline{\sigma}^{p}. \tag{14}$$

Multiplication of Eq. (14) with $\underline{\underline{M}}^{*}$ and by using Eq. (11) yields

$$\underline{\bar{\sigma}} = \underline{\underline{C}}^{0} : \underline{\varepsilon} + \underline{\bar{\sigma}}^{p} \tag{15}$$

where $\underline{\bar{\sigma}}^{p}$ is the plastic stress in the virtual undamaged configuration. Eq. (15) shows that if plastic deformations are defined with respect to the undamaged configuration, calculations of resulting plastic stresses can be performed independently of damage effects. This results in a simple operator split for the numerical implementation [16] and is a major advantage of assuming strain equivalence. Energy equivalence would lead to coupled plastic and damage iterations.
The thermodynamic driving force $\underline{Y}$ related to the internal damage tensor $\underline{D}$ is derived by taking the partial derivative of the strain energy with respect to $\underline{D}$ [17]:

$$\underline{Y} = -\frac{\partial \psi}{\partial \underline{D}} = -\frac{1}{2}\underline{\varepsilon} : \frac{\partial \underline{\underline{C}}(D^*)}{\partial \underline{D}} : \underline{\varepsilon}. \tag{16}$$

3.4 Damage Evolution

Similar to classical plasticity a damage potential is defined [17, 18] that controls the occurrence of damage:

$$f_d = Y_{eq} - B \leq 0 \tag{17}$$

where Y_{eq} is an equivalent scalar measure of $\underline{Y}$ and B is the current damage threshold. An associative evolution of internal damage is used

$$\dot{\underline{Y}} = \Delta\lambda_d \frac{\partial f_d}{\partial \underline{Y}} = \Delta\lambda_d \frac{1}{2Y_{eq}} \underline{\underline{L}} : \underline{Y} \tag{18}$$

where

$$Y_{eq} = \sqrt{\frac{1}{2}\underline{Y} : \underline{\underline{L}} : \underline{Y}} \tag{19}$$

with $\underline{\underline{L}}$ originally being defined as a fourth order tensor function of the 2nd order damage tensor $\underline{D}$ to account for changes in damage surface shape [19] and the Lagrange multiplier $\Delta\lambda_d$. In the present work $\underline{\underline{L}}$ is assumed to be constant to perform a principal investigation of damage evolution during multiaxial loading of paperboard. Further experiments will be necessary to determine a meaningful damage surface as well as its evolution for an exemplary paperboard material.
By introducing the loading/unloading and consistency conditions as usually done in plasticity and relating B to an internal variable β by the simple relationship

$$B = B_c \beta \tag{20}$$

where B_c is a material constant, the Lagrange multiplier $\Delta\lambda_d$ is calculated as

$$\Delta\lambda_d = \frac{\frac{1}{2Y_{eq}} \underline{Y} : \underline{\underline{L}} : \frac{\partial \underline{Y}}{\partial \underline{\varepsilon}}}{B_c - \frac{1}{2Y_{eq}} \underline{Y} : \underline{\underline{L}} : \frac{\partial \underline{Y}}{\partial \underline{D}} : \frac{\partial f_d}{\partial \underline{Y}}} : \dot{\underline{\varepsilon}}. \tag{21}$$

Finally, the damage tangent stiffness (assuming $\dot{\underline{\sigma}}^p = 0$) yields

$$\dot{\underline{\sigma}} = \left[\underline{\underline{C}}(D^*) + \underline{\varepsilon} : \frac{\partial \underline{\underline{C}}(D^*)}{\partial \underline{D}} : \frac{\partial f_d}{\partial \underline{Y}} \otimes \left(\frac{\partial f_d}{\partial \underline{Y}} : \frac{\partial \underline{Y}}{\partial \underline{\varepsilon}} \right) \right] : \dot{\underline{\varepsilon}}. \tag{22}$$

3.5 Viscous Regularization

To scale the damaged area to a more realistic width and reduce the mesh dependency, a Perzyna-type regularization is performed [24]. The damage evolution is given as

$$\dot{\underline{D}} = \eta < f_d > \frac{\partial f_d}{\partial \underline{Y}} \tag{23}$$

where $< \blacksquare >$ denote the Föppl bracket and η is the viscosity parameter. Written in incremental form Eq. (23) is written as

$$\Delta \underline{D} = \eta < f_d > \Delta t \frac{\partial f_d}{\partial \underline{Y}} \equiv \Delta\lambda_d \frac{\partial f_d}{\partial \underline{Y}} \tag{24}$$

where the corresponding Lagrange multiplier is introduced together with the residual [25]

$$r = \frac{\Delta\lambda_d}{\eta \Delta t} - f_d \tag{25}$$

that is used within a Newton-Raphson iteration scheme to compute all required increments. The algorithm is given in section **3.6**.

A simple example is presented to illustrate the regularizing effect of the present approach. Fig. 2 shows the sample modelled with shells (**ELFORM** = 2) under uniaxial tension (see also Fig. 4 for the mesh). One element was weakened ($A/A_0 = 0.90$) to achieve local softening.
Fig.3 shows the results for implicit calculations of the bar example for different pseudo-viscosities. A low viscosity parameter retards damage initiation and leads to higher damage values over the whole bar (see η_1 and η_2). It must be pointed out that viscous damage regularization highly depends on the used time scale and the corresponding parameters must be determined specifically for each calculation, as can be seen for η_3 to η_5 in Fig. 3. Here the high viscosity retards the damage evolution in a way that during the calculation time the weakened element won't be damaged completely. Further increase of viscosity leads to less damage when the termination time is reached.

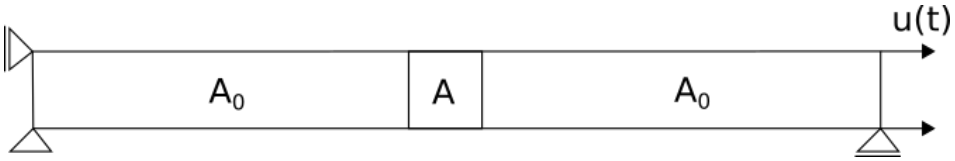

Fig. 2: Illustration of the bar example used with viscous regularization.

The damage initiation threshold was set to zero for the numerical study because the impact of damage evolution on the bulge test simulation result is investigated. A quantitative representation of the exact damage levels necessitates the determination of a damage surface for paperboard based on

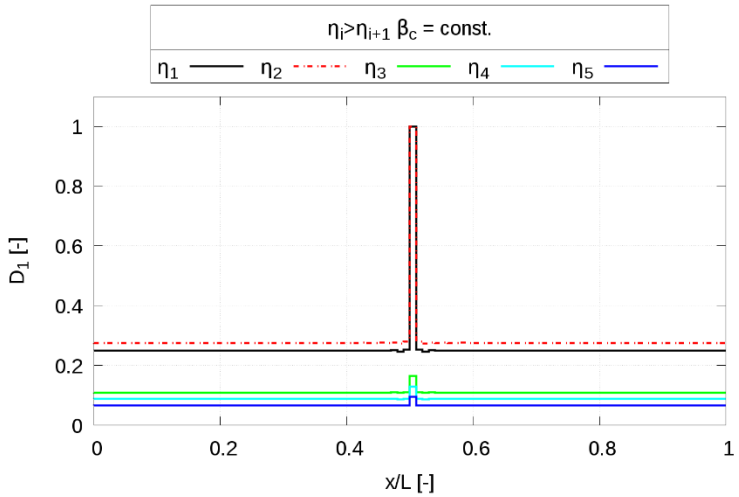

Fig. 3: Damage evolution for different pseudo-viscosities.

damage evolution measurements for different loading situations which is beyond the scope of the present work. Fig. 4 shows a contour plot of the damage variable D1 of the deformed bar for $\eta = \eta_1$.

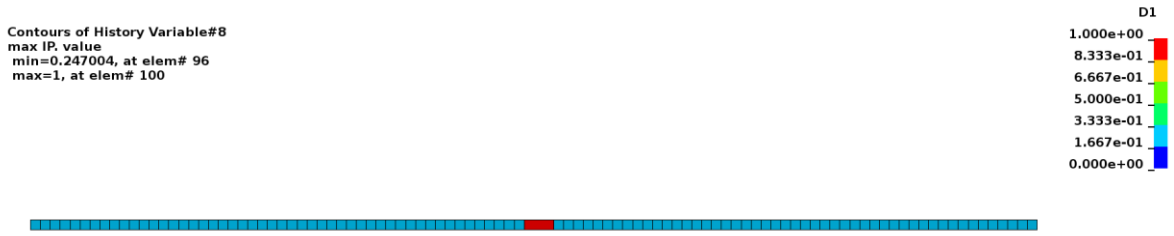

Fig. 4: Exemplary bar fringe level of D1 for $\eta = \eta_1$ as shown in Fig. 3.

To obtain a more physically motivated approach for the introduction of damage, non-local quantities can be used [13]. As a modified global calculation is necessary, these models require a more sophisticated implementation as e.g. ***MAT_NONLOCAL**.

3.6 Numerical Treatment

The presented 2nd order damage approach is included in a user material subroutine in LS-DYNA by using a Newton-Raphson iteration scheme for implicit time integration. The iteration procedure is described schematically in Box 1. An operator split is used so that the plastic and damage iteration can be performed separately.

Box 1: Viscous damage iteration.

1. Trial state:

$$\underline{D}_{n+1}^{trial} = \underline{D}_n, \qquad \beta_{n+1}^{trial} = \beta_n, \qquad \Delta\lambda_d = 0$$

2. Check damage potential:

$$f_d = Y_{eq}(\underline{\varepsilon}_{n+1}, \underline{D}_{n+1}^{trial}) - \left(B_0 + B_c\beta_{n+1}^{trial}\right)$$

IF: $f_d \leq 0$

$$\text{Set } (\blacksquare)_{n+1} = (\blacksquare)_{n+1}^{trial} \text{ and EXIT}$$

END IF

3. Compute residuals:

$$a = -\underline{D}_{n+1}^{trial} + \underline{D}_n + \Delta\lambda_d \frac{\partial f_d}{\partial \underline{Y}}, \qquad r = \frac{\Delta\lambda_d}{\eta\Delta t} - f_d$$

IF: $a \leq limit \;\&\&\; \mathrm{r} \leq limit$

$$\text{Set } (\blacksquare)_{n+1} = (\blacksquare)_{n+1}^{trial} \text{ and EXIT}$$

END IF

4. Compute increments:

$$\delta\lambda_d = \frac{-r + \frac{\partial f_d}{\partial \underline{D}} : \underline{\underline{X}}^{-1} : a}{\frac{1}{\eta\Delta t} - \frac{\partial f_d}{\partial \underline{D}} : \underline{\underline{X}}^{-1} : \frac{\partial f_d}{\partial \underline{Y}} - \frac{\partial f_d}{\partial \beta}}, \qquad \underline{\underline{X}} = \underline{\underline{1}} - \Delta\lambda_d \frac{\partial f_d}{\partial \underline{Y} \partial \underline{D}}$$

5. Update:

$$\beta_{n+1}^{trial} = \beta_{n+1}^{trial} + \delta\lambda_d, \qquad \Delta\lambda_d = \Delta\lambda_d + \delta\lambda_d, \qquad \underline{D}_{n+1}^{trial} = \underline{D}_{n+1}^{trial} + \underline{\underline{X}}^{-1} : \left(a + \delta\lambda_d \frac{\partial f_d}{\partial \underline{Y}}\right)$$

GOTO **3.**

4 Experimental Setup

Bulge tests with identic parameters to the numerical simulations were conducted. The test rig which is schematically depicted in Fig. 5 was developed by Huttel and Post [23]. In Fig. 5 a) the initial state and in Fig. 5 b) the state immediately before breakage is depicted. For a clear illustration, pneumatic cylinders and further test rig parts are not illustrated. Furthermore, the used optical measurement system GOM Aramis® is schematically depicted. To determine the elongations inline a stochastic pattern is required on the paperboard's surface. Tests with and without the sprayed on pattern were conducted to investigate if the pattern influences the mechanical properties. Since both the pressure and the elongation at failure were identical with and without the pattern, any influence of the pattern on the mechanical properties can be excluded. In the detailed section in Fig. 5 a) a membrane beneath the paperboard is shown. The membrane is used to separate the porous paperboard from the pressurized air. To avoid any influence by the membrane the Young´s Modulus is significantly smaller (4 MPa) compared to paperboard (2000 to 7000 MPa).

Per definition no material flow from the clamping is allowed. Therefore, a circumferential bead with a rough surface was provided in the clamping. Like in the numerical simulations the pressure increase is set to 0.1 bar/s.
To account for material inhomogeneities a representative area around the point of maximum displacement is evaluated and the average MD and CD strain is computed.

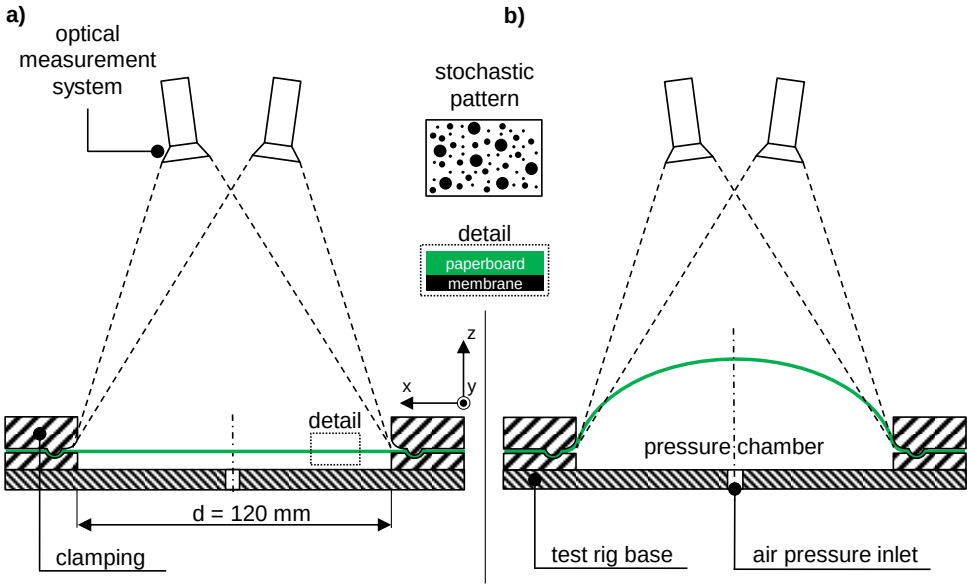

Fig. 5: Bulge test setup. a) Initial state, b) state immediately before fracture.

5 Results and Discussion

The final damage distribution for the chosen set of parameters is presented in Fig. 6 for the bulge simulation. The resulting strains in bulge experiments are shown in Fig. 7 together with simulation results using ***MAT_PAPER** and the present model with and without including damage effects.

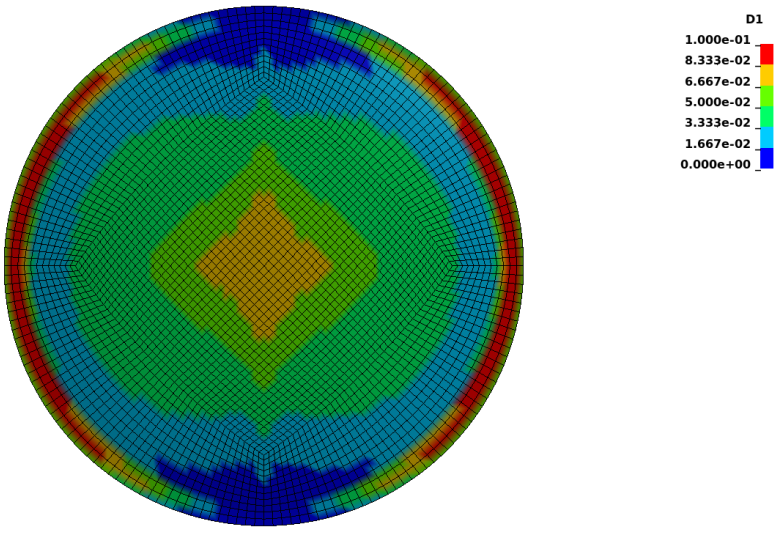

Fig. 6: Damage distribution in bulge simulation.

From literature [26] it is known that a sudden increase in damage is present before rapture and the pre-rupture damage is of a moderate amount. It is assumed that most of the damage effects immediately before rupture are a localized phenomenon and do not influence the measured strain average significantly. Under these assumptions most of the strain is a result of plastic effects and softening effects have only moderate impact on the simulation results, as illustrated in Fig. 7. A

distinction between plasticity and damage effects for a complex material such as paperboard is difficult and the discussion here is restricted the simplified continuum representation of the material. Further experiments are necessary to determine the damage in bulge test experiments and refine the presented damage formulation. However, the present approach offers a tool to predict coupled damage and plasticity effects under complex loading without the need of non-local quantities. As already stated before it is important to point out that the viscous parameters must be chosen carefully.

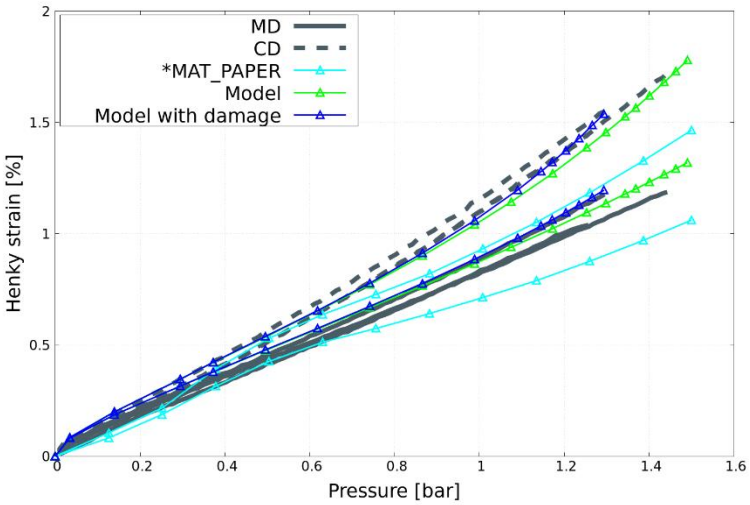

Fig. 7: Bulge test and simulation results. Damage distribution in bulge simulation.

6 Summary and Outlook

In the present work a modelling approach for the in-plane behaviour of paperboard was combined with CDM to investigate the influence of damage effects on bulge test simulations. The experimental results are represented well by the present approach, whereas **`*MAT_PAPER`**, that represents uniaxial tensile experiments well, was not able to represent the material behaviour in bulge experiments. It was found that most of the strain evolution can be contributed to plastic effects under the assumption that most of the damage evolution takes place just before material failure. To distinct damage and plastic effects for paperboard, elaborate experimental effort is necessary to enable for a prediction of material damage effects. A modification of the damage criterion is necessary for paperboard which will be the topic of further research.

7 Acknowledgement

The authors gratefully acknowledge financial support within the LOEWE program of excellence of the German Federal State of Hesse (project initiative "BAMP! Bauen mit Papier").

Literature

[1] Alava, M., Niskanen, K. “The physics of paper”. Reports on progress in physics, 69(3), (2006), 669.

[2] Tryding, J. “In-plane fracture of paper”. Doc. Thesis, 1996, Division of Structural Mechanics, Lund Institute of Technology, Sweden.

[3] Xia, Q. S., Boyce, M. C., & Parks, D. M. “A constitutive model for the anisotropic elastic–plastic deformation of paper and paperboard”. International journal of solids and structures, 39(15), (2002), 4053-4071.

[4] Mäkelä, P., Östlund, S. “Orthotropic elastic–plastic material model for paper materials”. International Journal of Solids and Structures, 40(21), (2003), 5599-5620.

[5] Nygårds, M., Just, M., & Tryding, J. “Experimental and numerical studies of creasing of paperboard”. International journal of solids and structures, 46(11-12), (2009), 2493-2505.

[6] Tjahjanto, D. D., Girlanda, O., Östlund, S. “Anisotropic viscoelastic–viscoplastic continuum model for high-density cellulose-based materials”. Journal of the Mechanics and Physics of Solids, 84, (2015), 1-20.

[7] Li, Y., Stapleton, S. E., Reese, S., Simon, J. W. “Anisotropic elastic-plastic deformation of paper: In-plane model”. International Journal of Solids and Structures, 100, (2016), 286-296.

[8] Karafillis, A. P., & Boyce, M. C. “A general anisotropic yield criterion using bounds and a transformation weighting tensor”. Journal of the Mechanics and Physics of Solids, 41(12), (1993), 1859-1886.

[9] Arramon, Y. P., Mehrabadi, M. M., Martin, D. W., Cowin, S. C. “A multidimensional anisotropic strength criterion based on Kelvin modes”. International Journal of Solids and Structures, 37(21), (2000), 2915-2935.

[10] Rowlands, R. E., Gunderson, D. E., Suhling, J. C., Johnson, M. W. “Biaxial strength of paperboard predicted by Hill-type theories”. The Journal of Strain Analysis for Engineering Design, 20(2), (1985), 121-127.

[11] Xia, Q. “Mechanics of inelastic deformation and delamination in paperboard”. Doc. Thesis, 2002, Massachusetts Institute of Technology.

[12] Madigan, D. "Prefabricated housing and the implications for personal connection." 18th Annual Pacific-Rim Real Estate Society Conference, 2012, 1-9.

[13] Isaksson, P., Hägglund, R., Gradin, P. “Continuum damage mechanics applied to paper”. International journal of solids and structures, 41(16-17), (2004), 4731-4755.

[14] Cordebois, J. P., Sidoroff, F. “Damage induced elastic anisotropy”. In Mechanical Behavior of Anisotropic Solids/Comportment Méchanique des Solides Anisotropes (pp. 761-774), (1982), Springer, Dordrecht.

[15] Chaboche, J. L. “Damage induced anisotropy: on the difficulties associated with the active/passive unilateral condition”. International Journal of Damage Mechanics, 1(2), (1992), 148-171.

[16] Simo, J. C., Ju, J. W. “Strain- and stress-based continuum damage models-I. Formulation”. International Journal of Solids and Structures, 23(7), (1987), 821-840.

[17] Murakami, S., Hayakawa, K., Liu, Y. “Damage evolution and damage surface of elastic-plastic-damage materials under multiaxial loading”. International Journal of Damage Mechanics, 7(2), (1998), 103-128.

[18] Murakami, S. "Continuum Damage Mechanics: A Continuum Mechanics Approach to the Analysis of Damage and Fracture". Dordrecht: Springer, 2012.

[19] Hayakawa, K., Murakami, S. “Thermodynamical modeling of elastic-plastic damage and experimental validation of damage potential”. International Journal of damage mechanics, 6(4), (1997), 333-363.

[20] Chow, C. L., Wang, J. “A finite element analysis of continuum damage mechanics for ductile fracture”. International Journal of Fracture, 38(2), (1988), 83-102.

[21] Borgqvist, E., Lindström, T., Tryding, J., Wallin, M., & Ristinmaa, M. “Distortional hardening plasticity model for paperboard”. International journal of solids and structures, 51(13), (2014), 2411-2423.

[22] Bažant, Z. P., & Jirásek, M. “Nonlocal Integral Formulations of Plasticity and Damage: Survey of Progress”. Journal of Engineering Mechanics, 128(11), (2002), 1119-1149.

[23] Post, P.-P., Huttel, D., Groche, P., Schabel, S. „Paper Characteristics Influencing the Deep Drawing Ability of Paper“. Progress in Paper Physics Seminar, Graz, (2011)

[24] Perzyna, P. “The constitutive equations for rate sensitive plastic materials”. Quarterly of applied mathematics, 20(4), (1963), 321-332.

[25] Wang, W. M., Sluys, L. J., & De Borst, R. “Viscoplasticity for instabilities due to strain softening and strain-rate softening”. International Journal for Numerical Methods in Engineering, 40(20), (1997), 3839-3864.

[26] Isaksson, P., Gradin, P. A., & Kulachenko, A. „The onset and progression of damage in isotropic paper sheets”. International Journal of Solids and Structures, 43(3-4), (2006), 713-726.